Chall. Nano Micro Scale Sci. Tech., 9(2):100-108, Summer and Autumn 2021
DOI: 10.22111/CNMST.2021.38360.1208

ORIGINAL RESEARCH PAPER

Multi-Objective Optimization of Frost Formation in Micro Channel Heat Sinks with Circular Fins Considering Microfluidic Effects

Hamed Safikhani [1,*], Mohsen Alaeian [1,2] and Alireza Fazlali [3]

[1] Department of Mechanical Engineering, Faculty of Engineering, Arak University, Arak 38156-88349, Iran
[2] Department of Mechanical Engineering, DEM/PEM – Politécnica/COPPE Federal University of Rio de Janeiro – UFRJ Caixa Postal: 68503, Cidade Universitária, Rio de Janeiro, RJ, 21941-972, Brazil
[3] Department of Chemical Engineering, Faculty of Engineering, Arak University, Arak 38156-88349, Iran

Received 28 April 2021; revised 11 September 2021; accepted 11 September 2021;

ABSTRACT: In this paper, multi objective Pareto optimization of frost formation in Micro Channel Heat Sink (MCHS) with circular fins with square and triangular configurations is performed in three steps. In the first step, the fluid flow is solved numerically in a number of MCHS using CFD techniques. In numerical modeling, basic equations of humid air and frost, including continuum, momentum, energy and phase change mechanism are numerically solved. Flow type is transient and the microfluidic regime is slip flow. In the second step, CFD data is used to model the objective functions namely volume fraction of ice and the heat transfer in MCHS using GMDH type artificial neural networks. The accuracy of GMDH modeling of objective functions is investigated using different statistical models. Finally, polynomials extracted from the GMDH are used to multi-objective optimization of frost formation in MCHS using NSGA II algorithm. In this step, the Pareto front, which contains very useful information in the design of MCHS containing frost formation, will be extracted and deeply discussed. In the results section, points with unique features are introduced. It will be shown that the design information presented in the results about MCHS containing frost formation can only be extracted with a multi-objective optimization approach.

KEYWORDS: *MCHS, microchannel, frost formation, CFD, slip regime, microfluidic, MOO.*

INTRODUCTION

Frost formation is a renowned phenomenon in HVAC, aeronautical and refrigeration industries. Frost mounting on the heat exchanger surfaces, causing higher thermal resistance and also it blocks the air path. Both phenomena decrease energy efficiency of the system. Frost naturally is a porous media with packs of the air trapped in the ice matrix. Therefore, it possesses a marked thermal resistance. The presence of frost in the heat exchanger's channels causes pressure drop with narrowing down the path of the air. In the process of the frost formation, humid flows pass coolant surface and mass transfer of steam present in the wet flow to the ice crystals when the air is saturated. This causes thicker frost and higher freezing density. Many researchers already have studied frost formation by numerical and experimental approaches. Hayashi et al. [1] was one of the pioneers who studied the growth of frost in three different time periods. The first period includes the primary initiation of the ice crystals which is quite short in comparison of the total time period. In this period frost does not grow markedly thick. Moreover, for this phase, it is not a porous media as it can be assumed as ice idols where convection heat and mass transfer are main growth mechanisms and diffusion to the frost sounds trivial. For the second period known as frost growth phase, frost is a porous media where molecular diffusion of the water vapor is dominant.

*Corresponding Author Email: *h-safikhani@araku.ac.ir*
Tel.: +989120686211; Note. This manuscript was submitted on April 28, 2021; approved on September 1.

Mass flow of the water vapour contributed in both increasing the density of the frost as well as growing it.

Finally, in the complete growth period of the frost, the temperature of the freezing surface reaches to water triple-point temperature. Therefore, a cyclic process starts where compressed water vapor diffuses through the frost and gradually freezes due to internal temperature gradient. Aoki et al. [2] thoroughly investigated this phase. Modeling frost formation can be classified in analytical models and computational fluid dynamics (CFD) based models. Analytical models generally assume the growth of the frost in only one direction. Tao et al. [3,4] proposed a model for mass transfer in frost layer. Lee et al. [5,6] presented a uni-dimensional model for simulating growth in frost density and thickness and also they developed a model for analyzing frost layer and air flow. Using averaging local volume method Le Gall et al. [7] introduced the relative equilibrium to anticipate frost growth. Na and Webb [8-10] suggested a model based on density of supersaturated water vapor in the frost layer. Yang et al. [11] found an effective model to prognosticate the performance of the fin-tube heat exchanger. Recently, Hermes et al. [12] developed a mathematical model which could accurately predict the frost thickness with a 10% discrepancy with experimental results. Kandula [13,14] proposed novel equations for frost over the straight surface and investigated the effect of different ambient parameters on frost characteristics.

Nomenclature

cp	specific heat capacity	y	vector of observations
D	mass diffusivity coefficient		**Greek Letters**
Q	heat transfer	ε	porosity
t	time	λ	thermal conductivity
T	temperature	μ	dynamic viscosity
u	velocity in x direction	v	velocity in y direction
V	velocity	ρ	density
w	velocity in z direction		**Subscripts**
x,y	spatial variables	a	air
x	vector of input parameters	f	frost
		ef	efficiency

Micro-channel heat exchangers are very efficient compact exchangers. Their benefit in comparison with fin-tube exchangers includes lower volume and weight and higher efficiency. They also possess lower internal space which decreases refrigeration load of the heat exchanger and potentially decreases the contribution in global warming with lower possible leakage of the refrigerant [15]. Lately, micro-channel heat exchangers are prevalent in HVAC systems. These heat exchangers are increasingly applied in chillers especially thermal pumps where they should work in wet and freezing condition. Shao et al. [16] studied a model with distributed micro-channel heat exchangers used in commercial thermal pumps to analyze the frost over the fin-tube evaporators. Moallem et al. [17,18] investigated the effect of surface temperature, surface coating and water blockage on the freezing performance of the micro-channel heat exchangers. Surface temperature was more important than surface coating and water blockage over frost growth speed and freezing time. Some other studies focused on the frost-defrost cycle of the heat exchangers which is very vital in designing thermal pump systems. Xia et al. [19] studied five different louvered-fin micro-channel heat exchangers and found that condensed droplets dramatically influence the pressure drop and heat transfer in recurring freezing cycles. Zhang and Hrnjak [20] studied the freezing performance of the micro-channel heat exchangers with parallel-flow parallel-fin (PF2) horizontal flat tubes. In comparison with conventional serpentine fins, the freezing performance was improved which is attributed to the superior permeability of the PF2 heat exchangers. Tso et al. [21] developed a distribution model taking into account the non-uniform distribution of the wall and air temperature in the coil to anticipate dynamic behavior of the finned-tube heat exchanger for both frost and non-frost conditions.

Wu et al. [22] studied the frost properties of a micro-channel heat exchanger with louvered-fin and derived the equation for the thickness of the frost. In recent years, Zhu et al. [23, 24] concentrated on increasing thermal transfer through the concept of reconstruction of developed thermal layers. This study included some parallel longitudinal micro-channels with some transverse channels. The transverse channels were used to divide the length of the flow into some independent streams. They found that computed hydraulic and thermal boundary layers were readily improved due to the shorter total length of the divided streams within the micro-channel. It was also reported that the pressure drop and also heat transfer improved in divided micro-channels in comparison with conventional micro-channels. In another similar study Cheng [25] analyzed the flow and heat transfer of a double accumulated micro-channel using some micro-processor. The effect of height of the fin's wall to the height of the micro-channel was examined. They found their superior performance compared to the conventional micro-channels. The evaluation of the 3D micro-channels divided with the transverse micro-pores was followed by Chai et al. [26] using experimental and numerical methods. They found the pressure drop and heat transfer for different conditions and geometries of rectangular walls in transverse micro-pores. Wang and Li [27] numerically simulated flow field in micro-channels with triangular walls in transverse micro-pores. Their parametric studies eventuated in an optimized micro-channel with promising performance. Hajmohammadi et al. [28] investigated the slip regime in microchannel heat sinks with one phase flow. They finally compared the the results with the related results without slip regime.

To achieve the optimal thermal behaviors in MCHS in frost formation, a multi-objective optimization (MOO) approach should be used to discover the best possible design points with appropriate heat transfer and frost formation. NSGA II algorithm is one of the best and most complete multi-objective optimization algorithms, which will be used in this paper as well. This algorithm was first proposed by Deb et al. [29], and it has been used in recent years in various engineering-related applications [30-33]. More over in recent years, some researchers have investigated different aspects in micro channels [34-36].

To the best of author's knowledge, there has been no study focusing on the multi-objective optimization of the frost formation in micro channels with circular fins considering the micro-fluidic effects in slip regime. In this paper, multi objective Pareto optimization of frost formation in interrupted Micro Channel Heat Sink (MCHS) with circular fins is performed using combination of CFD, GMDH type ANNs and NSGA II algorithm.

DEFINING THE DESIGN VARIABLES AND OBJECTIVE FUNCTIONS

The geometry investigated in this paper is schematically illustrated in Fig. 1. As shown in this figure in both square and triangular configurations, a number of parallel domains have been placed next to each other and formed a MCHS. Since, in this MCHS, the flow field in each computational domain is the same, the governing equations have been numerically solved for one domain and finally, the amount of heat transfer from total MCHS have been multiplied by the number of domains to get the total values. The total heat transfer (W) for the set of MCHS is computed as follows:

$$Q_{tot} = nq_1 \tag{1}$$

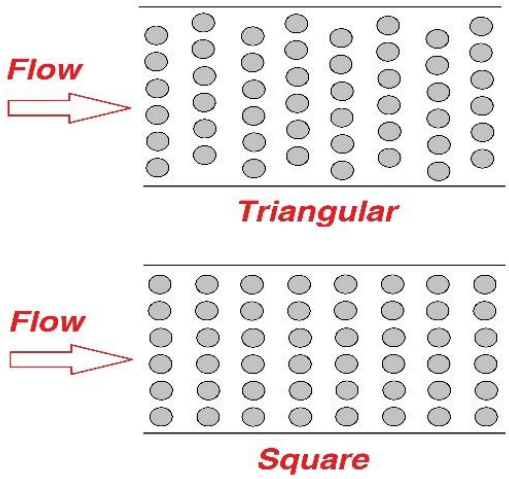


Fig. 1. Schematic view of MCHS with circular fins in triangular and square configurations.

The number of the set of MCHS is computed as follows:

$$n = \frac{W}{2V} \tag{2}$$

In the present study there are two independent geometrical design variables as shown in Fig. 2. The variation range of each one is shown in Table 1.

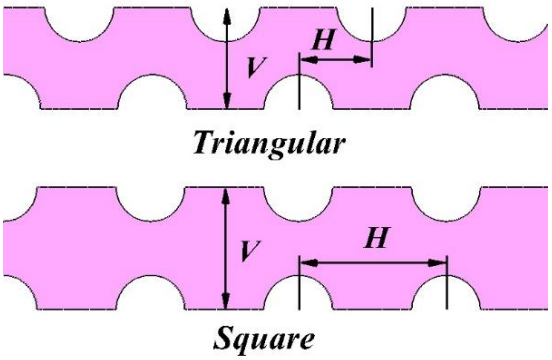


Fig. 2. Design variables in optimization process.

Table 1
Design variables and their range of variations.

Design Variables		From	To
Square	H (μm)	5	30
	V (μm)	30	60
Triangular	H (μm)	1	35
	V (μm)	30	60

As shown in this table each design variable is defined in five levels. By changing the design variables according to the Table 1, various designs will be created and simulated by CFD. Then, two polynomials can be generated using the GMDH type neural networks which will be further used for Pareto based multi objective optimization of MCHS with circular fins. Two conflicting objective functions are: maximizing the heat transfer and minimizing the ice volume fraction produced in MCHS.

MATHEMATICAL MODELING

Governing equations

In the present CFD modeling it is assumed that humid air is treated as an incompressible Newtonian fluid in laminar flow and density (ρ_a), mass diffusivity coefficient (D_a) and specific heat capacity (c_{pa}) of air are constant. Natural convection is negligible in both humid air and frost. Moreover, the humid air within the frost layer is considered saturated [13]. The continuity, 2D momentum, energy and mass transport equations are as follows:

$$\frac{\partial \rho_a}{\partial t} + \frac{\partial (\rho_a u)}{\partial x} + \frac{\partial (\rho_a v)}{\partial y} = 0 \tag{3}$$

$$\frac{\partial (\rho_a u)}{\partial t} + \frac{\partial (\rho_a u.u)}{\partial x} + \frac{\partial (\rho_a v.u)}{\partial y} = -\frac{\partial P}{\partial x} + \frac{\partial}{\partial x}\left(\mu \frac{\partial u}{\partial x}\right) + \frac{\partial}{\partial y}\left(\mu \frac{\partial u}{\partial y}\right) \tag{4}$$

$$\frac{\partial (\rho_a v)}{\partial t} + \frac{\partial (\rho_a u.v)}{\partial x} + \frac{\partial (\rho_a v.v)}{\partial y} = -\frac{\partial P}{\partial y} + \frac{\partial}{\partial x}\left(\mu \frac{\partial v}{\partial x}\right) + \frac{\partial}{\partial y}\left(\mu \frac{\partial v}{\partial y}\right) \tag{5}$$

$$\frac{\partial (\rho_a T)}{\partial t} + \frac{\partial (\rho_a u.T)}{\partial x} + \frac{\partial (\rho_a v.T)}{\partial y} = \frac{\partial}{\partial x}\left(\frac{\lambda_a}{c_{p,a}} \frac{\partial T}{\partial x}\right) + \frac{\partial}{\partial y}\left(\frac{\lambda_a}{c_{p,a}} \frac{\partial T}{\partial y}\right) \tag{6}$$

$$\frac{\partial (\rho_a w)}{\partial t} + \frac{\partial (\rho_a u.w)}{\partial x} + \frac{\partial (\rho_a v.w)}{\partial y} = \frac{\partial}{\partial x}\left(\rho_a D_a \frac{\partial w}{\partial x}\right) + \frac{\partial}{\partial y}\left(\rho_a D_a \frac{\partial w}{\partial y}\right) \tag{7}$$

Using an energy balance for a differential frost volume in the interior of the frost layer, energy equation can be expressed as:

$$\frac{\partial(\rho_f T)}{\partial t} = \frac{\partial}{\partial x}\left(\frac{\lambda_f}{c_{p,f}}\frac{\partial T}{\partial x}\right) + \frac{\partial}{\partial y}\left(\frac{\lambda_f}{c_{p,f}}\frac{\partial T}{\partial y}\right) + \frac{q_{sub}}{c_{pf}}\frac{\partial \rho_f}{\partial t} \quad (8)$$

For the densification rate of frost layer, the equation proposed by Na and Webb [9] has been used:

$$\frac{\partial \rho_f}{\partial t} = \frac{\partial}{\partial x}\left(\rho_a D_{ef}\frac{\partial w}{\partial x}\right) + \frac{\partial}{\partial y}\left(\rho_a D_{ef}\frac{\partial w}{\partial y}\right) \quad (9)$$

The viscosity and thermal conductivity are considered temperature dependent. The thermal conductivity of frost is commonly expressed as a function of frost density. In this study, it is used a correlation reported by Lee et al. [6]:

$$\lambda_f \left[{}^{W}/_{(m.K)}\right] = A_1 + A_2\rho_f + A_3\rho_f{}^2 \left[\rho \text{ in } {}^{kg}/_{m^3}\right] \quad (10)$$

where $A_1 = 0.132$ $A_2 = 3.13 \times 10^{-4}$ and $A_3 = 1.6 \times 10^{-7}$. The specific heat is defined as a function of frost density and porosity, as follows:

$$c_{p,f} = \frac{\left(c_{p,f}\rho_g(1-\varepsilon) + c_{p,a}\rho_a\varepsilon\right)}{\rho_f}. \quad (11)$$

The diffusive mass coefficient in the frost layer is determined as Na and Webb [8]:

$$D_{ef} = D_a\varepsilon^{\frac{1+\varepsilon}{2}}. \quad (12)$$

Boundary and initial conditions

For numerical simulation, the equations of previous sections should be solved subject to the related boundary and initial conditions. The schematic subjected boundary conditions are shown in Fig. 3. The fluid entered to the channel with known velocity and temperature (inlet) and exited with the known pressure (outlet). The fins are walls with known temperature lower than freezing temperature. The slip 1st order boundary conditions (0.001<Kn=0.05<0.1) are investigated for walls. This study models the frost layer growth period while the effects of crystal growth period are treated as initial conditions. Initial frost layer temperature is assumed to be constant and equal to the plate temperature, since the initial thickness is sufficiently thin.

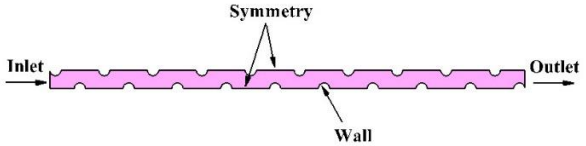


Fig. 3. The boundary conditions used in CFD simulations.

Numerical methods

The numerical simulation is performed using the finite volume method. A second order upwind method is used for the convective and diffusive terms and the SIMPLE algorithm is employed to solve the coupling between the velocity and pressure fields. To make sure that the obtained results are independent of the size and the number of generated grids, several grids with different sizes has been tested for each MCHS; and it has been attempted to consider for each MCHS the best grid, with the highest accuracy and the lowest computation cost. For an example of grid independency test (GIT), Table 2 shows the results of GIT for a MCHS. As it is shown in Table 2, except the MCHS with 5371 numbers of elements, increasing the grid numbers does not change significantly the VF and heat transfer of MCHS, hence the MCHS with 6512 numbers of elements is used. A sample of grid generation is shown in Fig. 4. Moreover, some operating conditions in numerical simulations are shown in Table 3.

Table 2
A sample of grid independency test results

Number of elements	VF (%)	q (MW)
5371	24.32	4.78
6512	28.51	5.29
7672	28.79	5.39
8571	28.99	5.42
9261	28.83	5.44

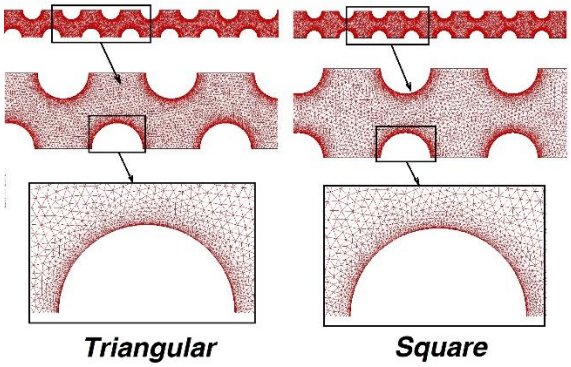


Fig. 4. A sample of grid generations.

Table 3
Some operating conditions in CFD simulations.

Parameter	Value
MCHS width (mm)	2.5
Inlet temperature (K)	275
Cold wall temperature (K)	260
Inlet velocity (m/s)	0.9
Kn	0.05
Time (min)	15
Relative Humidity (%)	60

VALIDATION

To validate the numerical model, its finding is compared with reliable results reported in related references. Since, there is neither experimental nor numerical study available

on the frost formation in micro channels considering microfluidic effect in slip regime each frost formation and microfluidic effect should be evaluated separately. Fig. 5(a) compared the results of frost formation in a conventional macro channel with that CFD data of Wu et al. [37]. As can be seen from Fig. 5(a), present modeling is able to accurately simulate the frost formation. The maximum and the mean numerical error in Fig. 5(a) are 8.2% and 5.1% respectively. Similarly, Fig. 5(b) shows the effect of slip effects in a micro-channel developed in this study with that of Hosseini et al. [38] with one phase which reveals great correlation using CFD. Similarly, the maximum and the mean numerical error in Fig. 5(a) are 9.01% and 4.7% respectively. Therefore, it can be said that presented model is accurate and reliable for simulation of frost formation in micro-channels considering microfluidic effects.

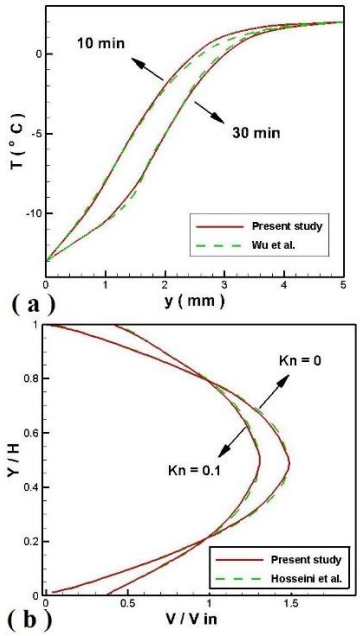


Fig. 5. a) Validation of frost formation results in a plane [37] **b)** Validation of microfluidic results in slip regime

GMDH MODELING RESULTS

Using the GMDH type neural network a model can be generated as a set of neural cells in which different pairs of them are connected in each layer through a quadratic polynomial and thus generated new nerve cells in the next layer. This view can be used in modeling to map inputs to outputs. The formal definition of the identification problem is to find a function $\hat{f}$ so that can be approximately used instead of actual one, f in order to predict output $\hat{y}$ for a given input vector $X = (x_1, x_2, x_3, \dots, x_n)$ as close as possible to its actual output y. Therefore, given M observation of multi-input-single-output data pairs so that:

$$y_i = f(x_{i1}, x_{i2}, x_{i3}, \dots, x_{in}) \quad (i = 1,2, \dots, M) \tag{13}$$

It is now possible to train a GMDH type neural network to predict the output values $\hat{y}_i$ for any given input vector $X = (x_{i1}, x_{i2}, x_{i3}, x_{i3}, \dots, x_{in})$ that is:

$$\hat{y}_i = \hat{f}(x_{i1}, x_{i2}, x_{i3}, \dots, x_{in}) \ \ (i = 1,2, \dots, M) \tag{14}$$

The problem now is to determine a GMDH neural network to minimize the square of the difference between the actual and predicted one, that is:

$$\sum_{i=1}^{M} \left[\hat{f}(x_{i1}, x_{i2}, x_{i3}, \dots, x_{in}) - y_i\right]^2 \rightarrow min \tag{15}$$

General connection between inputs and output variables can be expressed by a complicated discrete form of the Volterra functional series in the form of

$$y = a_0 + \sum_{i=1}^{n} a_i x_i + \sum_{i=1}^{n} \sum_{j=1}^{n} a_{ij} x_i x_j + \sum_{i=1}^{n} \sum_{j=1}^{n} \sum_{k=1}^{n} a_{ijk} x_i x_k + \cdots \tag{16}$$

Where is known as the Kolmogorov-Gabor polynomial. This complete form of mathematical description can be formed by a partial quadratic polynomial system consisting of only two variables (neurons):

$$\hat{y} = G(x_i, x_j) = a_0 + a_1 x_i + a_2 x_j + a_3 x_i x_j + a_4 x_i^2 + a_5 x_j \tag{17}$$

In this study, the Response Surface Methodology (RSM) which is a sub method of Design of Experiments (DOE) is used for designing the number of CFD data. There is a total number of 54 input-output CFD data considering seven design variables and two objective functions. Samples of CFD data are shown in Table 4. The GMDH type ANN will be used for such input-output data to find the polynomial model of MCHS.

In order to genetically design such GMDH type neural network described in previous section a population of 40 individuals with a crossover probability of 0.7 and mutation probability of 0.07 has been used in 200 generation that no further improvement has been achieved for such population size. In order to demonstrate the predictive power of GMDH-evolved neural networks, CFD data have been divided into two different sets, the training and testing sets. The training set which consists of 20 out of 25 inputs-output data pairs is used for training the GMDH models using the evolutionary method of this paper. The testing set which consists of 5 unforeseen input-output data samples during the training process is merely used for testing to show the prediction ability of such evolved GMDH type neural network models during the training process.

Table 4
Samples of numerical results using CFD.

No.	Square				Triangular			
	Design Variable		Objective Functions		Design Variable		Objective Functions	
	$H(\mu m)$	$V(\mu m)$	VF (%)	q (MW)	$H(\mu m)$	$V(\mu m)$	VF (%)	q (MW)
1	5	30	18.01	2.21	1	60	20.19	5.32
2	11.25	45	33.78	4.58	9.5	52.5	22.20	3.87
3	17.5	60	20.11	1.20	35	45	11.28	2.01
…								
25	30	52.5	28.51	5.29	18	30	13.91	1.71

A sample of good behavior of such GMDH type neural network models is illustrated in Fig. 6. It is evident from Fig. 6 that the evolved GMDH type neural network in terms of simple polynomial equations successfully model and predict the output of the testing data that have not been used during the training process. To view the accuracy of GMDH models, two statistical measures are presented in Table 5. These two statistical values are based on R^2 as absolute fraction of variance and *MAPE* as Mean Absolute Percentage of Error which are defined as follows:

$$R^2 = 1 - \sum_{i=1}^{n} \frac{(Y_{i\,ANN} - Y_{i\,CFD})}{Y_{i\,CFD}^2} \tag{18}$$

$$MAPE = (\frac{1}{n} \sum_{i=1}^{n} \frac{(Y_{i\,AMN} - Y_{i\,CFD})}{Y_{i\,CFD}} \times 100 \tag{19}$$

It is clear from Table 5 that the GMDH polynomials fits well the set of observations.

MULTI OBJECTIVE OPTIMIZATION RESULTS

In order to evaluate the optimal geometry of MCHS with circular fins as defined in Table 1, the GMDH models obtained in Section 4 are now used in a multi-objective optimization method using NSGA II algorithms. In all runs a population size of 60 has been chosen with crossover probability *Pc* and mutation probability *Pm* as 0.7 and 0.07 respectively. The two conflicting objective functions in this paper are *VF* and *q* that are optimized with respect to the design variables shown in Fig. 2 and Table 1. Fig. 7 shows the optimal non-dominant design points as Pareto front. In each configuration, there are five optimum design points, namely, *A, B, C, D* and *E* whose design variables and objective functions are shown in Table 6. It is clear from Fig. 7 that all the optimal design points in the Pareto front are non-dominated and could be selected by a designer as optimum MCHS. Obviously, choosing a better value for each objective function versus Pareto front would be a worse value for another objective. For better understanding the flow field in five extracted optimal points, the contour of ice volume fraction and velocity in each configuration are shown in Figs. 8-11 respectively.

In Fig. 8, the design points *A* and *E* stand for the best *VF* and the best *q* respectively. Moreover, the other optimum design points, *B* and *D* can be simply recognized from Fig. 8. At these two points, the changes in the objective functions in one direction are much greater than in the other. Points *B* and *D* which known as break points can only be identified by the multi-objective optimization approach used in this paper.

It is now ideal to find optimal design points that are compatible with both functions. This can be achieved by the method employed in this study, namely, the mapping method [30, 31]. In this method, the values of objective functions of all Pareto points are mapped range 0 and 1. Using the sum of these values for each Pareto point, the trade-off point simply is one having the minimum sum of those values. As a result, optimum design point *C* (in both configurations) is the trade-off points which have been obtained from this method.

In a post CFD investigation, the design points of the Pareto front obtained by the GMDH are re-evaluated by CFD. The results of such CFD analysis re-evaluations have been compared with those of numerical results using the GMDH model in Table 7. As seen the GMDH data agree well with the CFD results with error less than 5%. This shows the accuracy of the optimization process from start to end.

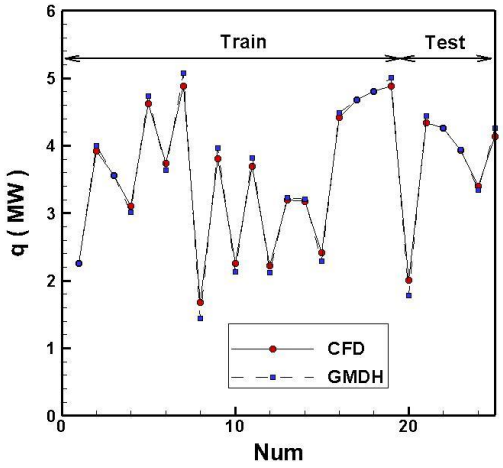


Fig. 6. A sample of comparison of predicted by GMDH and simulated by CFD (heat transfer).

Table 5
Amount of R^2 and MAPE for volume of frost (*VF*) and heat transfer (*q*).

Parameter	Square		Triangular	
	VF	*q*	*VF*	*q*
R^2	0.941	0.950	R^2	0.941
MAPE (%)	0.318	0.296	MAPE (%)	0.318

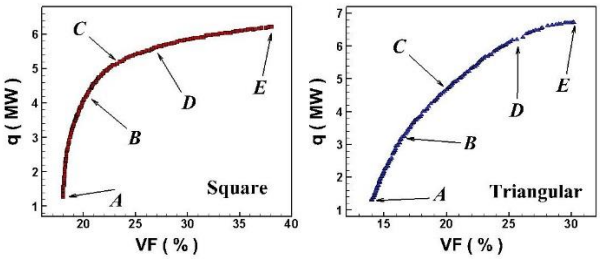


Fig. 7. Pareto front: square (left) triangular (right).

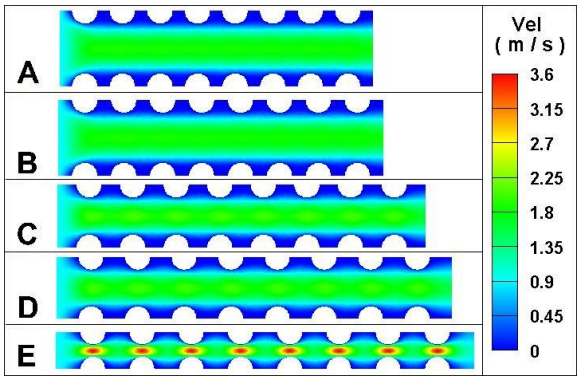


Fig. 8. Contour of humid air velocity related to five optimal points derived from Pareto front in square configuration.

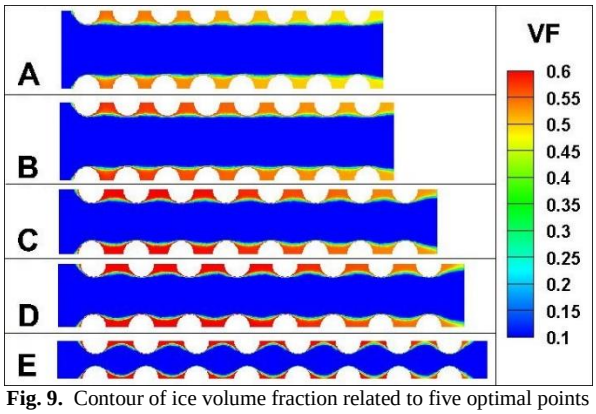


Fig. 9. Contour of ice volume fraction related to five optimal points derived from Pareto front in square configuration..

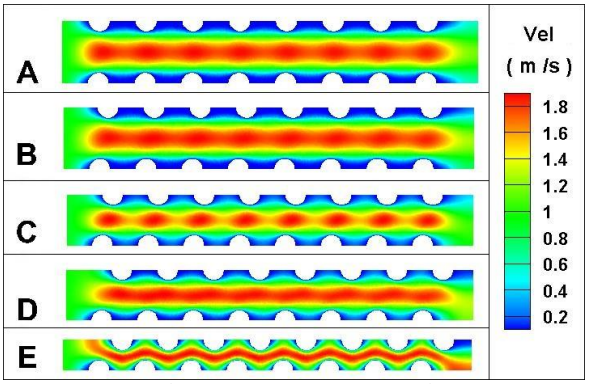


Fig. 10. Contour of humid air velocity related to five optimal points derived from Pareto front in triangular configuration.

The Pareto front obtained from the GMDH type ANNs model (Fig. 8) is mounted with the corresponding CFD simulation results in Fig. 11. From this figure it is clear that such a Pareto front is the best possible combination of CFD data target values, which shows the effectiveness of this paper, both in deriving the GMDH model and in obtaining the Pareto front.

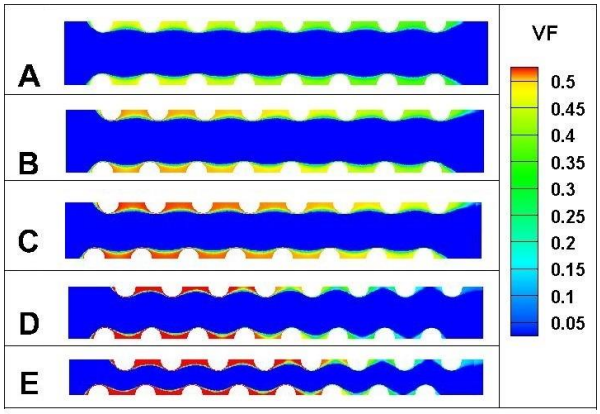


Fig. 11. Contour of ice volume fraction related to five optimal points derived from Pareto front in triangular configuration.

Table 7
Re-evaluation of the obtained optimal Pareto front using CFD.

Point		*VF (%)*			*q (MW)*		
		GMDH	CFD	Error (%)	GMDH	CFD	Error (%)
Triangular	*A*	14.13	13.69	-3.19	1.32	1.35	2.84
	B	14.27	14.43	1.11	1.87	1.92	3.10
	C	21.23	21.84	2.80	4.01	4.19	4.32
	D	28.57	29.74	3.94	5.51	5.35	-2.98
	E	29.99	30.54	1.82	6.71	6.44	-4.15

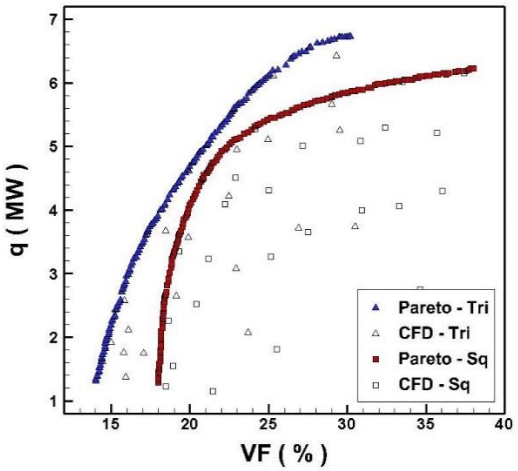


Fig. 12. Overlay of both Pareto fronts versus CFD data.

CONCLUSION

In this paper, multi objective Pareto optimization of frost formation in Micro Channel Heat Sink (MCHS) with circular fins with square and triangular configurations was performed in three steps. In the first step, the fluid flow was solved numerically in a number of MCHS using CFD techniques. In numerical modeling, flow type was transient and the microfluidic regime was slip flow. In the second step, CFD data was used to model the objective functions namely volume fraction of ice and the heat transfer in MCHS using GMDH type artificial neural networks. The accuracy of GMDH modeling of objective functions was investigated using different statistical models. Finally, polynomials extracted from the GMDH were used to multi-objective optimization of frost formation in MCHS using NSGA II algorithm. In this step, the Pareto front, which contains very useful information in the design of MCHS containing frost formation, would be extracted and deeply discussed. In the results section, points with unique features were introduced. It would be shown that the design information presented in the results about MCHS containing frost formation can only be extracted with a multi-objective optimization approach.

REFRENCES

[1] Hayashi Y, Aoki A, Adachi S, Hori K. Study of frost properties correlating with frost formation types, J. Heat Transfer. 1977; 99: 239-245.

[2] Aoki K, Katayama K, Hayashi Y. A study on frost formation: the process of frost formation involving the phenomena of water permeation and freezing, Bulletin of JSME. 1983; 26: 87-93.

[3] Tao YX, Besant R, Rezkallah K. Modeling of frost formation in a fibrous insulation slab and on an adjacent cold plate, International communications in heat and mass transfer. 1991; 18: 609-618.

[4] Tao YX, Besant R, Rezkallah K. A mathematical model for predicting the densification and growth of frost on a flat plate, International Journal of Heat and Mass Transfer. 1993; 36: 353-363.

[5] Lee KS, Kim WS, Lee TH. A one-dimensional model for frost formation on a cold flat surface, International Journal of Heat and Mass Transfer. 1997; 40: 4359-4365.

[6] Lee KS, Jhee S, Yang DK. Prediction of the frost formation on a cold flat surface, International Journal of Heat and Mass Transfer. 2003; 46: 3789-3796.

[7] Le Gall R, Grillot J, Jallut C. Modelling of frost growth and densification, International Journal of Heat and Mass Transfer. 1997; 40: 3177-3187.

[8] Na B, Webb RL. Mass transfer on and within a frost layer, International Journal of Heat and Mass Transfer. 2004; 47: 899-911.

[9] Na B, Webb RL. New model for frost growth rate, International Journal of Heat and Mass Transfer. 2004; 47: 925-936.

[10] Na B, Webb RL. A fundamental understanding of factors affecting frost nucleation, International Journal of Heat and Mass Transfer. 2003; 46: 3797-3808.

[11] Yang DK, Lee KS, Song S. Modeling for predicting frosting behavior of a fin–tube heat exchanger, International Journal of Heat and Mass Transfer. 2006; 49: 1472-1479.

[12] Hermes CJ, Piucco RO, Barbosa JR, Melo C. A study of frost growth and densification on flat surfaces, Experimental Thermal and Fluid Science. 2009; 33: 371-379.

[13] Kandula M. Frost growth and densification in laminar flow over flat surfaces, International Journal of Heat and Mass Transfer. 2011; 54: 3719-3731.

[14] Kandula M. Correlation of water frost porosity in laminar flow over flat surfaces, Special Topics & Reviews in Porous Media: An International Journal. 2012; 3: 79-87.

[15] Garimella S. Innovations in energy efficient and environmentally friendly space-conditioning systems, Energy. 2003; 28: 1593-1614.

[16] Shao LL, Yang L, Zhang CL. Comparison of heat pump performance using fin-and-tube and microchannel heat exchangers under frost conditions, Applied Energy. 2010; 87: 1187-1197.

[17] Moallem E, Padhmanabhan S, Cremaschi L, Fisher DE. Experimental investigation of the surface temperature and water retention effects on the frosting performance of a compact microchannel heat exchanger for heat pump systems, International Journal of Refrigeration. 2012; 35: 171-186.

[18] Moallem E, Cremaschi L, Fisher DE, Padhmanabhan S. Experimental measurements of the surface coating and water retention effects on frosting performance of microchannel heat exchangers for heat pump systems, Experimental Thermal and Fluid Science. 2012; 39: 176-188.

[19] Xia Y, Zhong Y, Hrnjak PS, Jacobi AM. Frost, defrost, and refrost and its impact on the air-side thermal-hydraulic performance of louvered-fin, flat-tube heat exchangers, International Journal of Refrigeration. 2006; 29: 1066-1079.

[20] Zhang P, Hrnjak PS. Air-side performance of a parallel-flow parallel-fin (PF2) heat exchanger in sequential frosting, International Journal of Refrigeration. 2010; 33: 1118-1128.

[21]Tso C, Cheng Y, Lai A. An improved model for predicting performance of finned tube heat exchanger under frosting condition, with frost thickness variation along fin, Applied Thermal Engineering. 2006; 26: 111-120.

[22]Wu J, Ouyang G, Hou P, Xiao H. Experimental investigation of frost formation on a parallel flow evaporator, Applied Energy, 2011. 88: p. 1549-1556.

[23] Xu J, Gan Y, Zhang D, Li X. Microscale heat transfer enhancement using thermal boundary layer redeveloping concept, International Journal of Heat and Mass Transfer. 2005; 48: 1662-1674.

[24] Xu J, Song Y, Zhang W, Zhang H, Gan Y. Numerical simulations of interrupted and conventional microchannel heat sinks, International Journal of Heat and Mass Transfer. 2008; 51: 5906-5917.

[25] Cheng Y. Numerical simulation of stacked microchannel heat sink with mixing-enhanced passive structure, International communications in heat and mass transfer. 2007; 34: 295-303.

[26] Chai L, Xia G, Zhou M, Li J, Qi J. Optimum thermal design of interrupted microchannel heat sink with rectangular ribs in the transverse microchambers, Applied Thermal Engineering. 2013; 51: 880-889.

[27] Wong KC, Lee JH. Investigation of thermal performance of microchannel heat sink with triangular ribs in the transverse microchambers, International communications in heat and mass transfer. 2015; 65: 103-110.

[28] Hajmohammadi MR, Alipour P, Parsa H. Microfluidic effects on the heat transfer enhancement and optimal design of microchannels heat sinks, International journal of heat and mass transfer. 2018; 126: 808-805.

[29] Deb K, Agrawal S, Pratap A, Meyarivan T. A fast and elitist multi-objective genetic algorithm: NSGA-II". IEEE Trans Evolutionary Computation. 2002; 6: 182-97.

[30] Safikhani H, Akhavan-Behabadi MA, Nariman-Zadeh, N, Mahmoodabadi MJ, Modeling and multi-objective optimization of square cyclones using CFD and neural networks, Chem. Eng. Res. Des, 2011. 89: 301-309.

[31] Safikhani H, Hajiloo A, Ranjbar MA. Modeling and multi-objective optimization of cyclone separators using CFD and genetic algorithms, Comput. Chem. 2011; 35: 1064–1071.

[32] Safikhani H, Abbassi A, Khalkhali A, Kalteh M. Multi-objective optimization of nanofluid flow in flat tubes using CFD, artificial neural networks and genetic algorithms, Adv. Powder Technol. 2014; 25: 1608-1617.

[33] Amanifard N, Nariman-Zadeh N, Borji M, Khalkhali A, Habibdoust A. Modeling and Pareto optimization of heat transfer and flow coefficients in micro channels using GMDH type neural networks and genetic algorithms, Energy Convers. Manage. 2008; 49: 311-325.

[34] Alibeigi M, Farahani SD. Effect of Porous Medium Positioning on Heat Transfer of Micro-channel with Jet, IJE TRANSACTIONS A: Basics. October 2020; 33(10): 2057-2064.

[35] Khosravi R, Rabiei S, Khaki M, Safaei MR. Entropy generation of graphene–platinum hybrid nanofluid flow through a wavy cylindrical microchannel solar receiver by using neural networks, Journal of Thermal Analysis and Calorimetry. 2021; 145: 1949–1967.

[36] Mohammadpour J, Sheikholeslami M, Masoudi M, Lee A. Optimization of nanofluid heat transfer in a microchannel heat sink with multiple synthetic jets based on CFD-DPM and MLA, International Journal of Thermal Sciences. septamber 2021; 167: 2021, 107008.

[37] Wu X, Chu F, Ma QS. Frosting model based on phase change driving force, International Journal of Heat and Mass Transfer. 2017; 110: 760-767.

[38] Hosseini SMJ, Soltani Goharrizi A, Abolpour B. Numerical study of aerosol particle deposition in simple andconverging–diverging micro-channels with a slip boundarycondition at the wall, Particuology. 2014; 13: 100–105.